

# Experiment and multiobjective optimization design of tape-spring hinges

Hui Yang · Rongqiang Liu · Yan Wang · Zongquan Deng · Hongwei Guo

Received: 21 February 2014 / Revised: 21 November 2014 / Accepted: 24 November 2014 / Published online: 14 December 2014  
© Springer-Verlag Berlin Heidelberg 2014

**Abstract** Flexible tape-spring hinges can be folded elastically and are able to self-deploy by releasing stored strain energy with fewer component parts and slight weights. This study presents a detailed investigation of the folding and deployment of single-layer tape-spring (SLTS) hinges and double-layer tape-spring (DLTS) hinges under pure bend loading. The material properties of tape-spring hinges are measured using an INSTRON machine. A DLTS hinge construction is created, and its moment-rotation relationship during quasi-static deployment is measured. An experiment is conducted to verify the validation of the numerical models for the DLTS hinges. The quasi-static deployment behavior of SLTS hinges and DLTS hinges is then analyzed using nonlinear finite element ABAQUS/Explicit solver, starting from the complete folded configuration. The DLTS hinge has good quasi-static deployment performances with regard to maximum stress ( $S_m$ ), steady moment ( $M^*$ ) and the peak moment ( $M_d$ ) during the DLTS hinge quasi-static deployment. In addition, the sampling designs of the DLTS hinges are created based on a three-level full factorial design of experiments (DOE) method. The surrogate models of  $S_m$ ,  $M^*$  and  $M_d$  of the DLTS hinges are derived using response surface method (RSM) to reduce the computational cost of quasi-static folding and deployment of numerical simulations. The Multiobjective optimization design (MOD) of the DLTS hinge is performed using modified non-dominated sorting genetic algorithm (NSGA-II) algorithm to achieve the optimal design. The finite element models for the optimal design based on numerical method are established to validate the optimization results.

**Keywords** Tape-spring hinge · Quasi-static deployment · Multiobjective optimization · Response surface method · Finite element analysis · Experiment

## 1 Introduction

Flexible hinges, which are folded elastically can self-deploy by releasing stored strain energy, which consist of a fewer component parts, can be manufactured conveniently. Flexible hinges have several advantages for space applications, including a low mass-to-deployed-stiffness ratio, cost, and self-latch. With the increasing demand, flexible hinges have been widely used as folding and deployment mechanisms in deployable structures, such as synthetic aperture radars (SARs), solar arrays and antenna booms. Tape-spring hinges have been used in the Japanese Mars orbiter PLANT-B for bar-like deployment structures of the thermal plasma analyzer (Oya and Onoda 2002).

Considerable efforts have been made to investigate the folding and deployment behaviors of flexible hinges through analytical, numerical, and experimental methods. Among those, some focused on various configurations methods, including single tape-spring (Mansfield 1973; Seffen and Pellegrino 1999; Seffen 2001; Seffen et al. 2000; Silver et al. 2005), single-layer pair tape-springs (Watt and Pellegrino 2002) and four pairs' tape-springs in a row (Boesch et al. 2008). Some researchers attempted to extend the tape-spring to larger structures by adopting monolithic structures, which included two omega-shaped thin metal shells that connect at the edges (Block et al. 2011) and two three-ply Kevlar sheets large tape-spring (Soykasap et al. 2008). In addition, the integral cylinder shell with parallel longitudinal slits has been shown to have good properties, such as easy manufacture and high stiffness (Marks et al. 2002; Silver et al. 2004; Yee and Pellegrino 2005). Yee (2006) conducted experiments

H. Yang (✉) · R. Liu · Y. Wang · Z. Deng · H. Guo  
State Key Laboratory of Robotics and System, Harbin Institute of  
Technology, Harbin, China  
e-mail: huiyang\_0431@163.com

and found that the integral flexible hinges could not resist angular momentum at the point of latching, which led to overshoot of the fully deployed configuration. Mobrem and Adams (2009) optimized the total stowed energy to control the dynamics of the deployment structures. Mallikarachchi and Pellegrino (2010) conducted optimization studies to find a flexible hinge design that can be folded by  $180^\circ$  with the shortest slot length and maximum strains after setting complete folding as the constraint. However, previous optimization studies may miss some optimal results because they just change the geometry parameters only at regular intervals. Moreover, the problems of the integral flexible hinges are the large folding moments that lead to hard folding before a spacecrafts launches, and high stress concentration after full deployment, which restrains the repeatability of the integral flexible hinges (Mallikarachchi and Pellegrino 2011). Compared with the integral flexible hinges, the flexible hinges consist of one or more pairs of tape-springs that possess smooth stress distribution. This type of tape-spring hinge can also improve the moment easily by increasing the layer of the tape-spring layer. However, the optimal configuration of the multi-layer tape-spring (MLTS) hinge is yet to be solved. The folding and deployment of the MLTS hinges involves a high nonlinear post-buckling and material contact process. Thus surrogate model techniques are employed in the nonlinear finite element analysis (FEA) for fast iteration, and response surface method (RSM) is chosen to derive the surrogate model for the MLTS hinges. The thin-walled tube hinge with double slots has been investigated (Yang et al. 2014) using the finite element (FE) method and RSM, but there is no experiment to valid and modify the numerical model.

This study aims to investigate quasi-static folding and deployment behaviors of the single-layer tape-spring (SLTS) hinges and the double-layer tape-spring (DLTS) hinges. The quasi-static folding and deployment of the flexible hinges are performed using ABAQUS/Explicit solver. An experiment apparatus is constructed to verify the developed numerical models before using them for further optimization study. When the tap-spring hinge begins to deploy, it must be fully folded first. As the relative rotation angle is increased and the end blocks move closer together, the moment remains approximately constant which is called as steady moment  $M^*$ . When the tape-spring hinges is closely to completely deployment, the centre part of the tape-spring hinge suddenly snaps through and the deformation locates in a short longitudinally curved region while the moment decreases quickly and reaches to a peak moment  $M_d$ . The objectives are set as  $M^*$  and  $M_d$  during the tape-spring hinge quasi-static deployment. Maximum stress ( $S_m$ ) during the complete hinge folding is set as the constraint condition. The separation distance  $s$  (i.e. the distance from the bottom to the top of the clamp holder end), the tape-spring section radius  $R$ , and central angle  $\varphi$  are considered as the three design variables. Quadratic

polynomial functions are employed to construct the response surface surrogate models of  $S_m$ ,  $M^*$ , and  $M_d$ . A three-level full factorial design of experiment (DOE) method is employed to plan the sampling points. The 27 sample design points, which are used to derive the response surface functions, are analyzed by ABAQUS/Explicit, and the modified non-dominated sorting genetic (NSGA-II) algorithm is used to solve the multiobjective optimization design problems.

## 2 Problem description

The structures considered in this study are the SLTS and the DLTS hinges, in which each tape spring layer in the DLTS hinge has the same configurations. All hinges have the same baseline geometry with a layer thickness of  $t=0.12$  mm, a total longitudinal length of  $L=126$  mm, and two clamp ends with lengths of  $b=20$  mm, which are applied to the clamp and fix the tape-springs in the folding and deployment experiments. For the DLTS hinge, the two tape-springs in the same side are closed tightly together. Both ends of both tape-springs are connected using rigid clamp holders and clamp covers. The complete structure and geometric parameters of the DLTS hinge are depicted in Fig. 1. The separations distance  $s$  is the inner arc trajectory vertex distance between two sets of the tape-springs. To simulate the quasi-static deployment of the tape-spring hinges, the finite element models are established to analyze the propertis of the hinges. And the experiment apparatus is also designed and used to verify the accuracy of the numerical method.

The hinge generated a steady moment  $M^*$  during quasi-static deployment that should be larger than a given value at any folding angle to ensure complete deployment, especially when the hinge deploys against resistive forces. And the peak moment  $M_d$  during quasi-static deployment should be less than a given value to avoid an excessive shock and overshoot in the case of the hinge at the end of deployment. Moreover, the concentrated stress  $S_f$  on the hinge should be small enough to increase repeated use times. Thus, three key quasi-static deployment behavior parameters are used to evaluate the performance of the hinges, maximum stress ( $S_m$ ) during the hinge quasi-static complete folding is selected as constraints, steady moment ( $M^*$ ), and peak moment ( $M_d$ ) of the hinge quasi-static deployment are selected as the two optimization objectives.

## 3 Quasi-static deployment

### 3.1 Material properties

The material of the tape-spring hinges is titanium-nickel alloy Ni36CrTiAl with a mass density of  $\rho=8.0 \times 10^3$  kg/m<sup>3</sup>, Poisson's ratio  $\nu=0.35$ . The material tension test is shown in

**Fig. 1** Complete structure and geometric parameters of the DLTS hinges

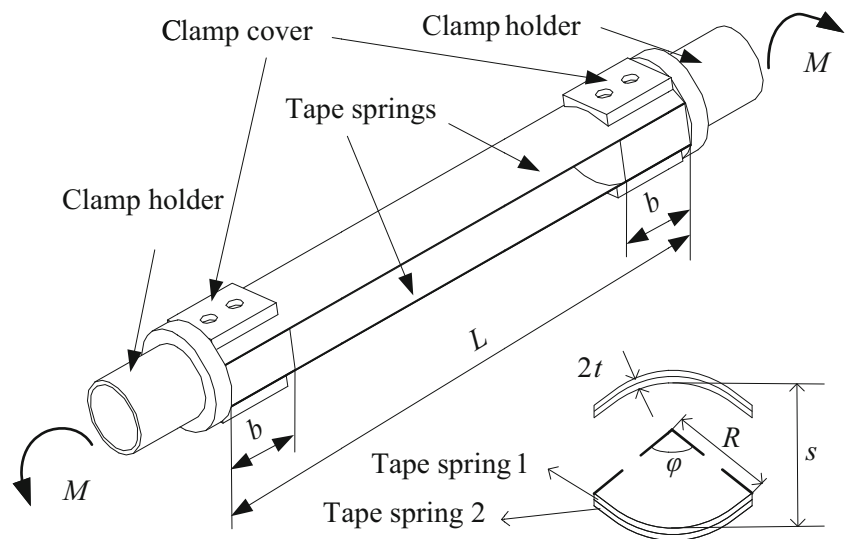


Fig. 2 and the tensile stress-strain curve measured using an INSTRON machine is plotted in Fig. 3. The range considered in defining Young’s modulus  $E$  is started from zero, which does not consider the initial part (0.005 strain). Yong’s modulus  $E$  is derived using linear fit method by choosing the linear range of the measured stress-strain data. And the fitted equation is obtained as follows:

$$y_s = 193.69 + 36939.98x_e \quad (1)$$

where  $y_s$  is the fitting tensile stress of Ni36CrTiAl and  $x_e$  is the measured strain. The slope of the linear fit function is  $E=36939.98$  Pa which approximately equals to  $E=36.94$  MPa. The fitted stress-strain curves of Ni36CrTiAl are shown in Fig. 3. The measured data is added to help the readers understand this paper as shown in Table 1 which are selected from the measured stress-strain data at a certain interval. It is shown

that the yield stress is  $\sigma_y=1.11$  GPa and the ultimate stress is  $\sigma_u=1.19$  GPa of the Ni36CrTiAl.

### 3.2 Numerical simulation

Folding and deployment simulations of thin-walled structures involve significant nonlinear processes, such as contact between different surfaces of the structures, buckling, and dynamic snaps. Convergence, numerical stability and singularity problems in the stiffness matrix (Yee and Pellegrino 2005; Seffen and Pellegrino 1999) were the main limits on the structural configurations with the implicit solver. The explicit solver applies the kinematic state of each of freedom through a direct integration of motion equations to avoid the problems. Thus, the finite element (FE) models are set up in the ABAQUS/Explicit with four nodes that are fully integrated to reduce shell elements (S4R) with an approximate element size of 3 mm. To simulate end rotation, the two reference nodes 1, and 2, located at each end are set as kinematic coupling constraints to either end surface. Reference node 1

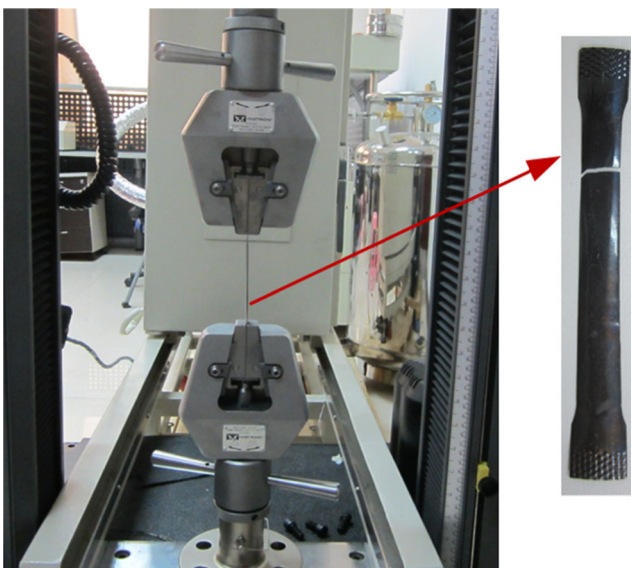


**Fig. 2** Experimental instrument of Ni36CrTiAl

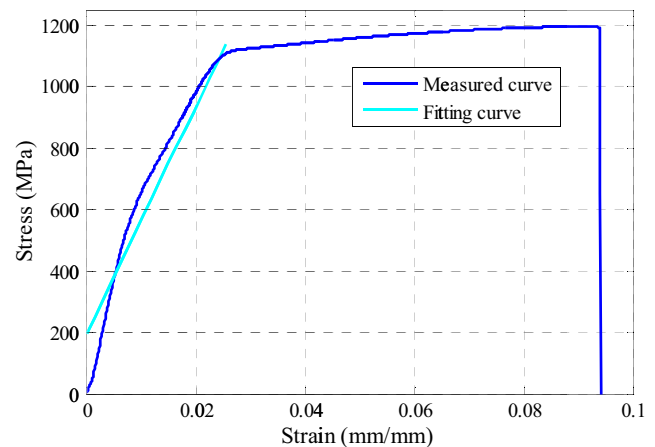


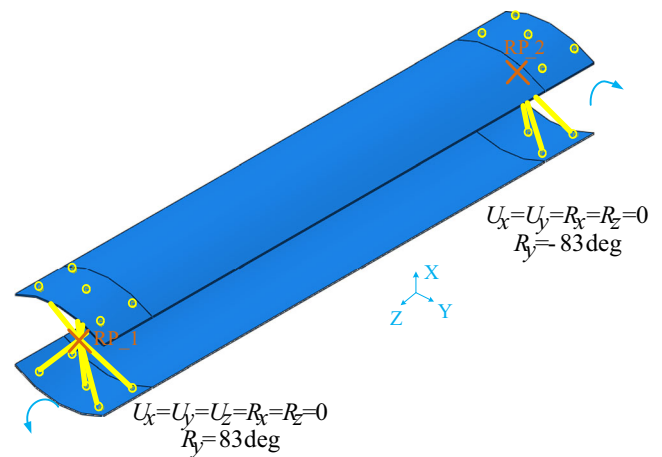
**Fig. 3** The measured and fitting stress-strain curves of Ni36CrTiAl

**Table 1** The tensile measured data of Ni36CrTiAl

| Stress (Mpa) | Strain (mm/mm) |
|--------------|----------------|
| 0.00003      | 0.20503        |
| 0.00159      | 80.60233       |
| 0.00214      | 129.6336       |
| 0.00225      | 138.8764       |
| 0.00303      | 205.2924       |
| 0.00392      | 281.0048       |
| 0.00503      | 367.8347       |
| 0.00625      | 460.2736       |
| 0.00692      | 505.6656       |
| 0.00858      | 589.29         |
| 0.01025      | 663.8018       |
| 0.0127       | 743.1121       |
| 0.01414      | 789.2793       |
| 0.01625      | 857.1693       |
| 0.0187       | 937.4854       |
| 0.02103      | 1010.47        |
| 0.02381      | 1079.93        |
| 0.02614      | 1111.36        |
| 0.03881      | 1138.93        |
| 0.05903      | 1171.07        |
| 0.08192      | 1192.10        |
| 0.08692      | 1194.03        |
| 0.09336      | 1192.96        |
| 0.09404      | 653.2091       |
| 0.09412      | -1.47172       |

(RP 1) is restrained of all freedom except for the rotation about the global  $y$ -axis, and reference node 2 (RP 2) is allowed to rotate about the  $y$ -axis as well as translate along the global  $z$ -axis, as shown in Fig. 4. The bending angle  $\alpha$  of the hinge is the sum of the rotational angle of the two reference nodes, i.e.,  $\alpha=166^\circ$ . To apply loads as smoothly as possible, Smooth-Step is employed when applying and removing loads. The general contact is assigned to the entire model to analyze the contact among the surfaces of DLTS hinge (Mallikarachchi and Pellegrino 2011).

The quasi-static folding simulation time is 1 s and imposes a rotation of  $\alpha=166^\circ$  by rotating the two reference nodes RP 1 and RP 2. The DLTS hinge is rotated back to its original configuration by an opposite variation of  $\alpha=-166^\circ$  to simulate deployment. A simulation step, in which both ends are held stationary, is added to dissipate the kinetic energy in the folded configuration before starting the deployment simulation. Quasi-static folding and deployment numerical simulation are conducted on the DLTS hinge with a separation distance of  $s=16$  mm. Each tape-spring section has a radius of  $R=18$  mm, a central angle of  $\varphi=76^\circ$ , a thickness of  $t=0.12$  mm, a longitudinal length of  $L=126$  mm, and a clamp end length of  $b=20$  mm. The energy variation for the DLTS hinge during quasi-

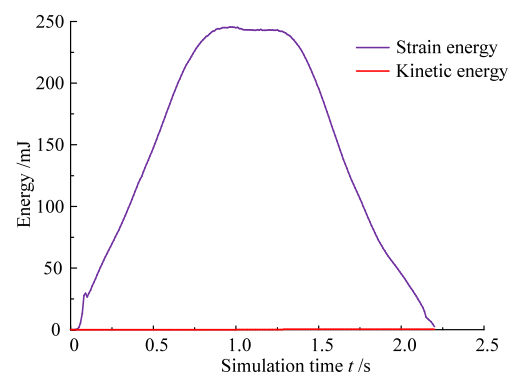
**Fig. 4** The boundaries for the DLTS hinge

static folding and deployment is shown in Fig. 5. The kinetic energy is lower than 10 % of the strain energy, which means that the simulation process is quasi static.

A complete moment-rotation relationship of the DLTS hinge in a quasi-static folding and deployment simulation cycle is shown in Fig. 6. The peak moment during quasi-static folding, which is required to fold the DLTS hinge, is higher than the peak moment of deployment, which is always characterized as a locking torque of a deployable mechanism. This behavior is attributed to the unstable post-buckling equilibrium path of the shell structures. The moment between snap through during quasi-static folding and snap back during quasi-static deployment is almost steady. The steady moment when the DLTS hinge starts to deploy is also considered as the driving moment of the deployable mechanisms. Meanwhile, the stress of the DLTS hinge is at maximum, which must decrease to improve the reusability of the tape-spring hinge.

### 3.3 Test procedure

The quasi-static deployment test system is designed and assembled to check the numerical models. The test system is composed of two computers, two digital multi-meters for measuring

**Fig. 5** Energy variation for the DLTS hinge during quasi-static folding and deployment

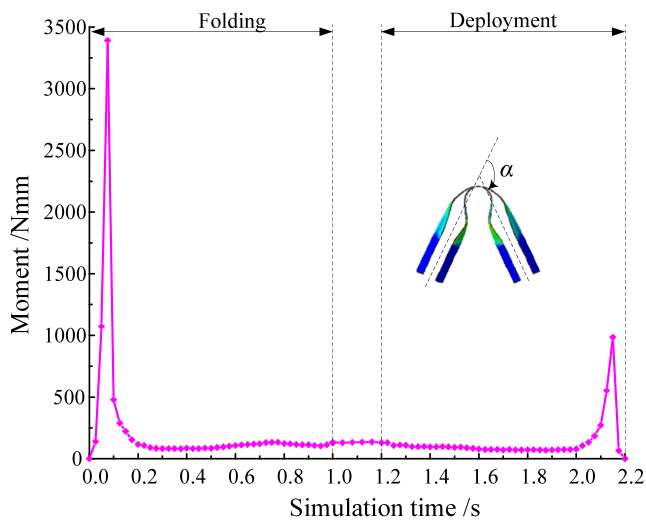


**Fig. 6** Complete moment-rotation relationship in a folding and deployment simulation cycle

rotation angles, two strain gauge digitizers that digitize the strain signal to the computers, and a test apparatus, as shown in Fig. 7. The test apparatus consists of two gear boxes with a reduction of 64. One gear box is attached to a guide rail, and the other is attached to a rigid foundation. These gear boxes support the strain gauges and angle sensors that can be seen on the left and right side views. The two ends of the DLTS hinge are fixed using two semi-circle holders that are connected to the shafts of the strain gauges.

The quasi-static experiment is conducted on the DLTS hinge with a separation distance of  $s=16$  mm. Each tape-spring section radius as a radius of  $R=18$  mm, central angle of  $\varphi=76^\circ$ , thickness of  $t=0.12$  mm, longitudinal length of  $L=126$  mm, and clamp end length of  $b=20$  mm. The geometric dimensions of the tape-spring section are the same as that of the numerical model. Rotations up to  $83^\circ$  are applied manually using two knobs and transferred to the hinge through the gear boxes. Before starting the test, the strain gauges and angle

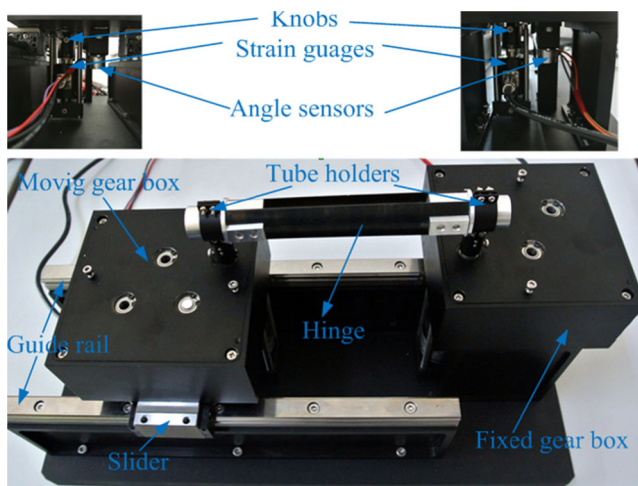


**Fig. 7** Detailed hinge quasi-static deployment test apparatus

sensor readings are calibrated to zero in the deployed configuration. The hinge is pinched in the middle and folded by rotating the two ends by an equivalent angle to avoid damage the DLTS hinge. In the test procedure the ends are rotated back by a few steps by spinning the two gear boxes with the desired amount while keeping the two end moments approximately equal. Afterward the moment and the rotation angle values are written down. A comparison of the DLTS hinge configuration during the quasi-static deployment is shown in Fig. 8. This qualitative comparison shows that the entire geometric configurations and the positions of the localized deformation regions in the DLTS hinge are in good accordance with each other. Meanwhile, the complete deployed configuration obtained from the numerical simulation has some residual stress on the hinge.

Moment-rotation curves are obtained by plotting the folding angle  $\alpha$ , which is compared with the numerical results, as shown in Fig. 9. The moment-rotation relationship of the

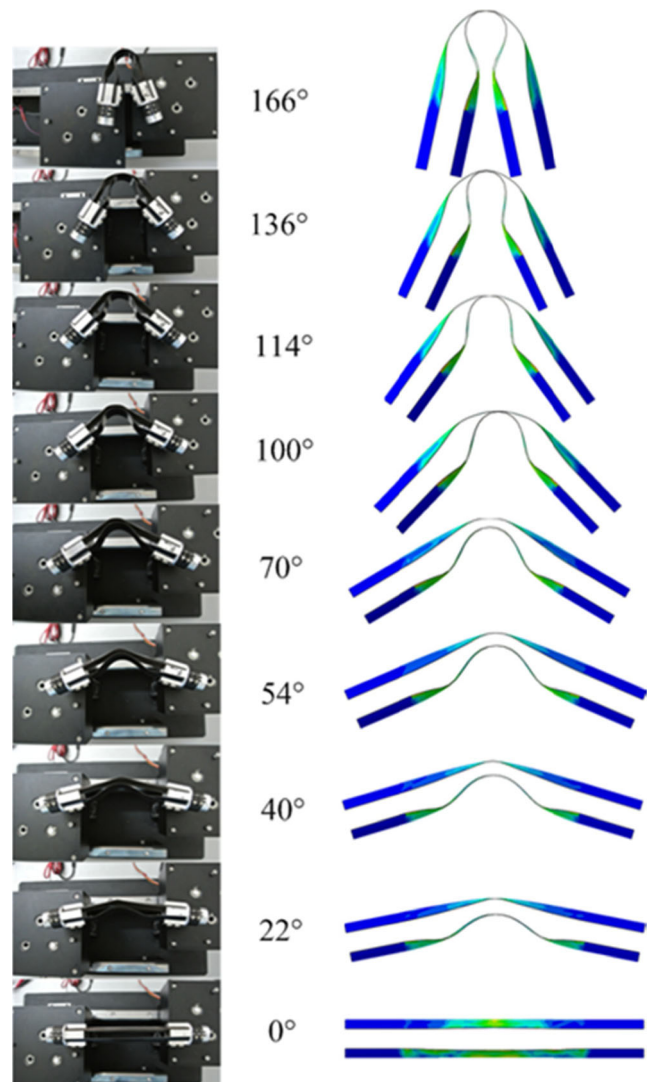


**Fig. 8** Comparison of the DLTS hinge configuration during quasi-static deployment

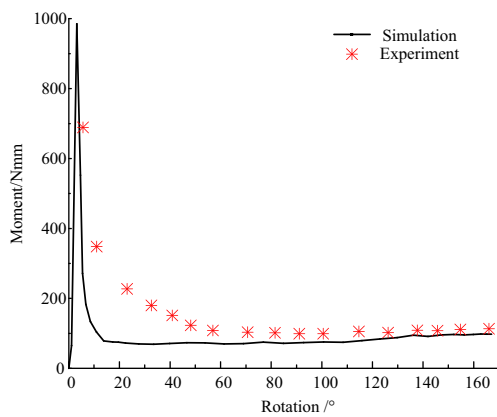


**Fig. 9** Compare of moment-rotation profiles during quasi-static deployment

DLTS hinge has a high nonlinear behavior during quasi-static deployment. The peak moment is reached when the snap through of the DLTS hinge occurs before the tape-springs of the hinge contact each other. The moment tends to steady as the rotation increases, and the steady moment will slightly increase as the contact regions of the localized fold between the tape springs increases. The numerical moments agree well with the measured moments from the fully folded configuration to the unfold configuration, corresponding to  $166^\circ$  and  $0^\circ$  rotations, respectively. The measured steady-state deployment moment with a large rotation has an average value of 104.62Nmm, whereas the numerical result is around 96.43Nmm. Furthermore, the main area of the quantitative discrepancy is the profile slope from the peak moment to the steady-state moment. This discrepancy can be attributed to that bolts, the rigid clamp ends and the rigid clamp holders enhance the bend stiffness of the DLTS hinges in the actual application, but these parts are deleted to simplify the numerical model and reduce the computational cost.

### 3.4 Numerical results comparison of two types of tape-spring hinge

In this study, the influences of tape-spring layer parameters on the response of the tape-spring hinge under pure bend loading are investigated. Using validated FE models, numerical analyses are first conducted to compare the

deployment performances of the two types of the tape-spring hinge, i.e., the SLTS and the DLTS hinge, under quasi-static pure bend loading. To investigate the influences of tape-spring layer on the  $S_m$ ,  $M^*$ , and  $M_d$  of the flexible hinges, SLTS and DLTS hinges of special tape-spring separations with a layer thickness of  $t=0.12$  mm are analyzed. The tape-spring section radius, the separation distance, and the tape-spring section central angle are listed in Table 2. The numerical results indicate that both  $M_d$  and  $M^*$  of the DLTS hinge are more than two times that of the SLTS hinge with the same tape-spring layer thickness of  $t=0.12$  mm. However, the  $S_m$  of the DLTS hinge is less than that of the SLTS hinge for all the tape-spring hinge configurations. These reasons are attributed to the fact that the contacts between the tape-spring layers can enhance the bending stiffness of the DLTS hinges. The configuration of the DLTS hinges shows better behaviors in both  $S_m$ ,  $M^*$ , and  $M_d$  under pure bend loading, compared with that of the SLTS hinges. Therefore, the DLTS hinge is selected as a better structural component in this study. The multiobjective optimization design (MOD) is employed to further improve the deployment behavior under pure bend loading.

## 4 Response surface models of DLTS hinges

The RSM of surrogate modeling technologies is widely employed in the optimization studies (Liu and Day 2008; Hou et al. 2012, 2014) to reduce the computational cost of quasi-static folding and deployment of nonlinear FEA. To date, the quasi-static deployment optimization of multilayer tape-spring hinges using RSM is unavailable.

### 4.1 Response surface method

RSM (Box and Wilson 1951) is a collection of mathematical and statistical techniques, applied in optimization problems and process development (Li et al. 2011; Qi et al. 2012). The surrogate models are modeled by using RSM to obtain the optimal quasi-static deployment behaviors of tape-spring hinges and reduce the computational cost.

**Table 2** The quasi-static deployment behavior indices for the hinges

| $s$ (mm) | $R$ (mm) | $\varphi$ (deg) | $S_m$ (GPa) |       | $M_d$ (Nm) |       | $M^*$ (Nm) |        |
|----------|----------|-----------------|-------------|-------|------------|-------|------------|--------|
|          |          |                 | DLTS        | SLTS  | DLTS       | SLTS  | DLTS       | SLTS   |
| 16       | 15       | 70              | 0.409       | 0.437 | 0.920      | 0.417 | 0.0813     | 0.0260 |
| 18       | 18       | 80              | 0.562       | 0.593 | 1.185      | 0.536 | 0.139      | 0.0471 |
| 20       | 21       | 90              | 0.595       | 0.608 | 1.185      | 0.550 | 0.221      | 0.0934 |

**Table 3** Step size and range of design variables of DLTS hinges

| Parameter                     | Step size | Lower bound | Upper bound |
|-------------------------------|-----------|-------------|-------------|
| Central angle $\varphi$ (deg) | 10        | 70          | 90          |
| Section radius $R$ (mm)       | 3         | 15          | 21          |
| Distance $s$ (mm)             | 2         | 16          | 20          |

In this study, the responses of the tape-spring are  $S_m$ ,  $M^*$ , and  $M_d$ , which can be written in terms of a series of basic functions:

$$\tilde{y}(x) = \sum_{i=1}^N \beta_i \varphi_i(x) \tag{2}$$

where  $\tilde{y}(x)$  is the responses of  $S_m(x)$ ,  $M^*(x)$ , and  $M_d(x)$ ,  $N$  is the number of the basic functions  $\varphi_i(x)$ ; and  $\beta_i$  is the coefficients of the basic functions. Every sample point consists of  $n$

**Table 4** Sample points and quasi-static deployment indices of DLTS hinges

| No. | $R$ /mm | $\varphi$ /deg | $s$ /mm | $S_m$ /GPa | $M^*$ /Nmm | $M_d$ /Nmm |
|-----|---------|----------------|---------|------------|------------|------------|
| 1   | 15      | 70             | 16      | 0.409      | 0.081      | 0.920      |
| 2   | 15      | 70             | 18      | 0.445      | 0.085      | 1.087      |
| 3   | 15      | 70             | 20      | 0.451      | 0.126      | 1.378      |
| 4   | 15      | 80             | 16      | 0.461      | 0.104      | 0.928      |
| 5   | 15      | 80             | 18      | 0.483      | 0.117      | 1.104      |
| 6   | 15      | 80             | 20      | 0.503      | 0.159      | 1.382      |
| 7   | 15      | 90             | 16      | 0.513      | 0.118      | 0.833      |
| 8   | 15      | 90             | 18      | 0.525      | 0.154      | 1.04       |
| 9   | 15      | 90             | 20      | 0.512      | 0.216      | 1.392      |
| 10  | 18      | 70             | 16      | 0.472      | 0.095      | 1.014      |
| 11  | 18      | 70             | 18      | 0.508      | 0.109      | 1.304      |
| 12  | 18      | 70             | 20      | 0.510      | 0.150      | 1.539      |
| 13  | 18      | 80             | 16      | 0.544      | 0.117      | 0.974      |
| 14  | 18      | 80             | 18      | 0.562      | 0.139      | 1.185      |
| 15  | 18      | 80             | 20      | 0.541      | 0.176      | 1.592      |
| 16  | 18      | 90             | 16      | 0.639      | 0.125      | 0.631      |
| 17  | 18      | 90             | 18      | 0.623      | 0.157      | 0.922      |
| 18  | 18      | 90             | 20      | 0.581      | 0.216      | 1.322      |
| 19  | 21      | 70             | 16      | 0.425      | 0.105      | 1.132      |
| 20  | 21      | 70             | 18      | 0.440      | 0.115      | 1.501      |
| 21  | 21      | 70             | 20      | 0.443      | 0.152      | 1.903      |
| 22  | 21      | 80             | 16      | 0.579      | 0.116      | 0.896      |
| 23  | 21      | 80             | 18      | 0.562      | 0.128      | 1.147      |
| 24  | 21      | 80             | 20      | 0.552      | 0.196      | 1.504      |
| 25  | 21      | 90             | 16      | 0.653      | 0.136      | 0.420      |
| 26  | 21      | 90             | 18      | 0.645      | 0.152      | 0.741      |
| 27  | 21      | 90             | 20      | 0.595      | 0.221      | 1.185      |

**Table 5** Accuracy of different RS models for DLTS hinges

|       | $R^2$ | $R^2_{adj}$ | $RMSE$  | RE interval (%) |
|-------|-------|-------------|---------|-----------------|
| $S_m$ | 0.977 | 0.965       | 0.01347 | [-3.31, 3.09]   |
| $M^*$ | 0.984 | 0.976       | 0.00618 | [-5.81, 5.69]   |
| $M_d$ | 0.987 | 0.980       | 0.04732 | [-5.42, 5.48]   |

dependable variables  $x_j$  ( $j=1, 2, \dots, n$ ). In this study, the quadratic polynomials are chosen to create the basic functions which can be written as

$$\begin{aligned} \tilde{y}(x) = & \beta_0 \\ & + \sum_{j=1}^n \beta_j x_j + \sum_{\substack{j=1 \\ (j < k)}}^n \beta_{jk} x_j x_k + \sum_{k=1}^n \beta_{kk} x_k^2 \end{aligned} \tag{3}$$

The regression coefficients of quadratic polynomials can be calculated using the least-square method:

$$b_f = (\Phi^T \Phi)^{-1} \Phi^T y \tag{4}$$

where  $b_f=(\beta_1, \beta_2, \dots, \beta_N)$ , and  $N$  is the number of basic function  $\varphi_i$ . The matrix  $\Phi$  consists of the following basic functions of  $M$  sample points:

$$\Phi = \begin{bmatrix} \varphi_1(x)_1 & \dots & \varphi_N(x)_1 \\ \vdots & \ddots & \vdots \\ \varphi_1(x)_M & \dots & \varphi_N(x)_M \end{bmatrix} \tag{5}$$

where  $\varphi_N(x)_M$  is the  $N$ th basic function of the  $M$ th design point, and  $M$  is the number of design points. The coefficient  $b$  can be determined by substituting Eqs. (5) into (4).

The accuracy of the responses should be evaluated with the use of several criteria, i.e., relative error (RE), coefficient of multiple determination ( $R^2$ ), root mean square error (RMSE),

**Table 6** The six added sample points

| No. | $R$ /mm | $\varphi$ /deg | $s$ /mm |
|-----|---------|----------------|---------|
| 1   | 15.5    | 72.5           | 16.5    |
| 2   | 16.5    | 75             | 17      |
| 3   | 17.5    | 77.5           | 17.5    |
| 4   | 18.5    | 82.5           | 18.5    |
| 5   | 19.5    | 85             | 19      |
| 6   | 20.5    | 87.5           | 19.5    |

**Table 7** The REs between numerical and RS models for the six added sample points

| No. | $S_m$      |            |       | $M^*$      |            |       | $M_d$      |            |       |
|-----|------------|------------|-------|------------|------------|-------|------------|------------|-------|
|     | FE results | RS results | RE %  | FE results | RS results | RE %  | FE results | RS results | RE %  |
| 1   | 0.445      | 0.450      | -1.03 | 0.0838     | 0.0885     | -5.65 | 1.085      | 0.981      | 4.57  |
| 2   | 0.524      | 0.502      | 4.18  | 0.105      | 0.101      | 3.05  | 1.124      | 1.071      | 4.56  |
| 3   | 0.538      | 0.543      | -1.83 | 0.120      | 0.116      | 3.55  | 1.186      | 1.137      | 4.14  |
| 4   | 0.553      | 0.586      | -6.04 | 0.156      | 0.149      | 4.14  | 1.204      | 1.203      | 0.05  |
| 5   | 0.563      | 0.600      | -6.63 | 0.162      | 0.171      | -5.43 | 1.097      | 1.212      | -6.84 |
| 6   | 0.580      | 0.602      | -3.92 | 0.185      | 0.194      | -5.06 | 1.260      | 1.196      | 5.13  |

and the adjusted coefficient of multiple determination ( $R^2_{adj}$ ), which can be written as

$$RE = \frac{\tilde{y}_i - y_i}{y_i} \tag{6}$$

$$R^2 = 1 - \frac{SSE}{SST} \tag{7}$$

$$R^2_{adj} = 1 - \frac{M-1}{M-N} (1-R^2) \tag{8}$$

$$RMSE = \left( \frac{SSE}{M-p-1} \right)^{0.5} \tag{9}$$

where  $y_i$  is the FEA results of the  $i$ th sample point,  $i$  is the response of the  $i$ th sample point,  $i=1, 2, \dots, M$ ,  $M$  is the

number of design points, and  $p$  is the number of non-constant terms in the response functions.  $SST$  and  $SSE$  represent the total sum of squares and the sum of squares of the residuals, respectively:

$$SST = \sum_{i=1}^M (y_i - \bar{y})^2 \tag{10}$$

$$SSE = \sum_{i=1}^M (y_i - \tilde{y}_i)^2 \tag{11}$$

where  $\bar{y}$  is the mean response of  $y_i$ .

For the RS model, the values of  $R^2$  and  $R^2_{adj}$  vary from 0 to 1, which is the correlation level between the FEA results and the responses. Thus, the larger  $R^2$  and  $R^2_{adj}$  are, the smaller  $RE$  and  $RMSE$  are, the better the Response Surface (RS) fitting is.

### 4.2 Sample points

To derive the surrogate models of  $S_m$ ,  $M^*$ , and  $M_d$ , FEA should be performed for a series of design points

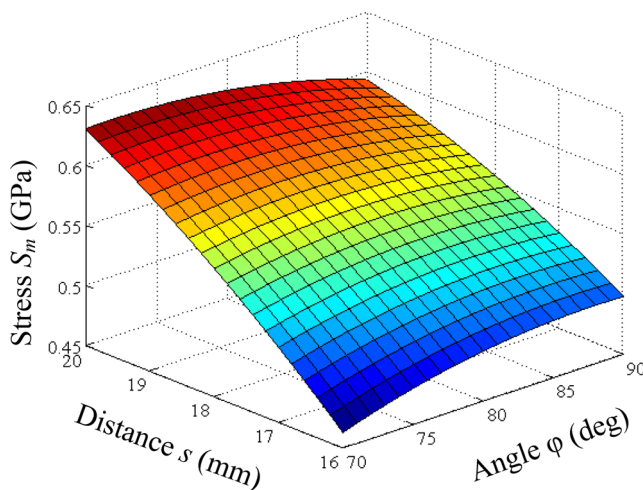


**Fig. 10** Response surfaces of  $S_m$  for DLTS hinge

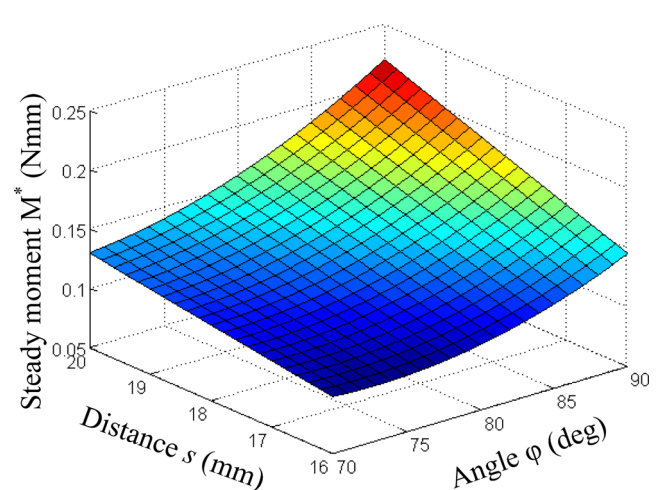


**Fig. 11** Response surfaces of  $M^*$  for DLTS hinges



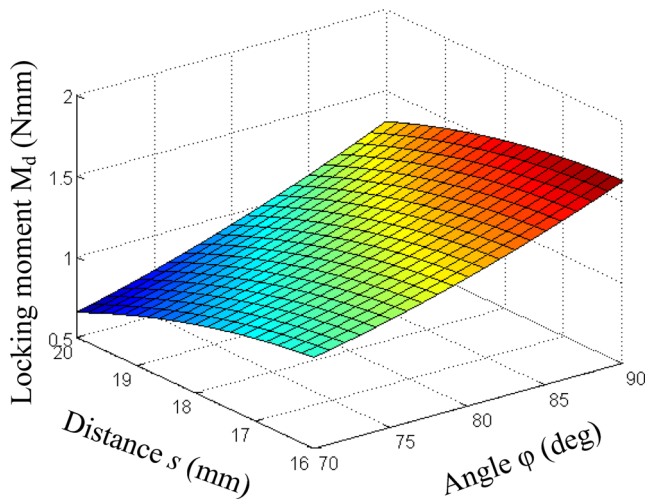


Fig. 12 Response surfaces of  $M_d$  for DLTS hinges

determined using DOE within the design domain. Some DOE methods, such as orthogonal arrays, central composite design, Latin hypercube, and full factorial are available (Lindman 1992). The three-level full factorial design is employed in this study, i.e., the central angle  $\varphi$  is changed from  $70^\circ$  to  $90^\circ$  with a typical interval of  $10^\circ$ , the section radius  $R$  is changed from 15 to 21 mm for every 3 mm and the separated distance  $s$  is increased from 16 to 20 mm with a typical interval of 2 mm. The responses of  $S_m$ ,  $M^*$ , and  $M_d$  of the DLTS hinges are derived at these 27 sample points. The range and step size of the central angle  $\varphi$ , section radius  $R$ , and tape-spring separation for the DOE are listed in Table 3. The coefficients of polynomial  $\beta_i$  are calculated from the FEA results using Eqs. (4) and (5).

The boundaries of the FE models are set as depicted in Section 3.2. The FEA results of the quasi-static deployment indices for the 27 design points are listed in Table 4.

### 4.3 RS models of DLTS hinges

On the basis on the methodology of the Section 4.2, the surrogate RS models for  $S_m$ ,  $M^*$ , and  $M_d$  prediction of the DLTS hinges with respect to design variable  $s$ ,  $\varphi$ , and  $R$  are derived from the DOE results, which are written as follows:

$$\begin{aligned}
 S_m = & -3.8324 + 0.02198\varphi + 0.1419R + 0.2093s - 0.002787s^2 \\
 & - (1.0175\varphi^2 + 47.05R^2 - 9.4707\varphi R + 8.9865\varphi s + 20.735Rs) \\
 & \times 10^{-4}
 \end{aligned}
 \tag{12}$$

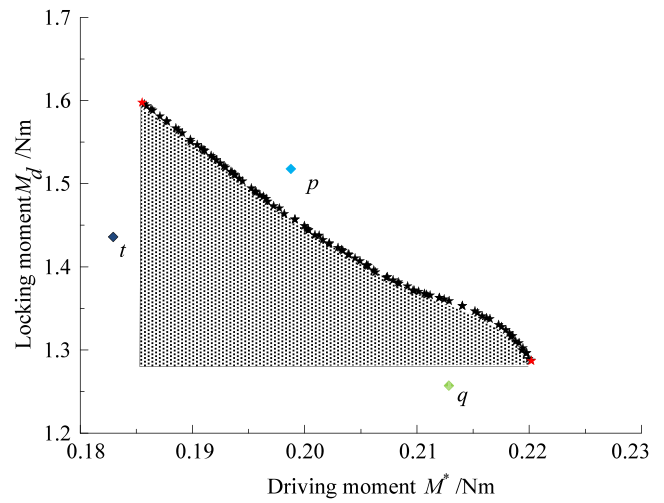


Fig. 13 Pareto fronts of  $M^*$  and  $M_d$  for the DLTS hinge with  $S_m \leq 0.6\text{GPa}$

$$\begin{aligned}
 M^* = & 1.3551 - 0.004534\varphi + 0.03062R - 0.1782s + 0.004136s^2 \\
 & + (3.06 \times 10^{-2} \varphi^2 - 5.1453R^2 - 1.61\varphi R + 5.332\varphi s + 2.0764Rs) \\
 & \times 10^{-4}
 \end{aligned}
 \tag{13}$$

$$\begin{aligned}
 M_d = & -4.9493 + 0.1683\varphi + 0.4018R - 0.5465s + 0.01223s^2 \\
 & - (0.644384\varphi^2 + 2.92R^2 + 5.740\varphi R - 1.102\varphi s - 9.408Rs) \times 10^{-3}
 \end{aligned}
 \tag{14}$$

The accuracy of the quadratic polynomial functions is evaluated by substituting the approximation of the responses obtained from Eqs. (12)–(14) and the FEA results into Eqs. (6)–(11), where  $M=27$  (number of design samples) and  $N=10$  (number of basic functions of the quadratic polynomial). The values of  $R^2$ ,  $R^2_{adj}$ ,  $RMSE$ , and  $RE$  are computed and shown in Table 5.  $R^2$ ,  $R^2_{adj}$  are sufficiently large, whereas  $RMSE$  and  $RE$  are sufficiently small. The factorial selection of the evenly distributed 27 design points over the entire design domain is therefore checked.

To verify the accurate over the entire design domain six sets of sample points, which are different from the 27 previous sample points, are chosen to analyze using the ABAQUS and calculate the accurate between the finite element (FE) results and the RS results. The added six sample points are shown in Table 6, and the REs between the numerical and surrogate models for the six added sample points are listed in Table 7. It is found that the REs are changed from  $-6.84\%$  to  $4.57\%$  which are no more than  $10\%$ . Thus the response surface is acceptably accurate.

The derived response surfaces for  $S_m$ ,  $M^*$ , and  $M_d$  of the DLTS hinge with a section radius of  $R=18$  mm are plotted in

**Table 8** Ideal optimums of the two single objective functions for the DLTS hinge

| Single objective | $s$ (mm) | $\varphi$ (deg) | $R$ (mm)  | $M^*$ (Nm) | $M_d$ (Nm) | $S_m$ (GPa) |
|------------------|----------|-----------------|-----------|------------|------------|-------------|
| Ideal $M^*$      | 20       | 89.999588       | 18.460642 | 0.2201998  | 1.2868293  | 0.5999992   |
| Ideal $M_d$      | 20       | 79.403441       | 20.999996 | 0.1855228  | 1.5974097  | 0.5294499   |

Figs. 10, 11 and 12, respectively.  $S_m$ ,  $M^*$ , and  $M_d$  favor different tape-spring section central angles and separated distances. Optimizing these two moment objectives simultaneously is often impossible. Thus, the modified NSGA-II algorithm for multiobjective optimization is selected to determine the trade-off hinge configurations under different design conditions.

### 5 Multi-objective optimization design (MOD) of DLTS hinges

#### 5.1 MOD approach and optimization algorithm

The DLTS hinges should be designed for the best quasi-static deployment performances under pure bend loading. To complete MOD, the steady moment, the peak moment and concentrated stress are chosen according actual engineering requirements. The driving moment  $M^*$ , i.e., the steady moment of quasi-static deployment that the DLTS hinge generates should be larger than 0.18 Nm to ensure full deployment, especially when the hinge deploys against some resistive forces. In addition, the locking moment  $M_d$ , i.e., the peak moment during quasi-static deployment that the DLTS hinge generates should be less than 1.6 Nm in order to avoid excessive shock and overshoot in the hinge at the end of deployment. Thus, two optimized objectives are chosen as driving and locking moments. Furthermore, the concentrated stress during quasi-static complete folding on the DLTS hinge should be smaller than 0.6GPa to increase the repeated use times, which is set as the constraint condition. The section central angle  $\varphi$ , separated distance  $s$ , and the section radius  $R$  of the tape-spring in the DLTS hinges are chosen as the design variables. The DLTS hinge length ( $L=126$  mm), tape-spring layer thickness ( $t=0.12$  mm), and clamp end length ( $b=20$  mm) are also set as constants in the design process. Therefore, MOD models of the DLTS hinge with

two quasi-static deployment design objectives can be written as follows:

$$\begin{cases} \text{Opt.}\{M^*(\varphi, R, s) \geq 0.18\text{Nm}, M_d(\varphi, R, s) \leq 1.6\text{Nm}\} \\ \text{S.t. } S_m(\varphi, R, s) \leq 0.6\text{GPa}; \\ 70^\circ \leq \varphi \leq 90^\circ; \\ 15 \text{ mm} \leq R \leq 21 \text{ mm}; \\ 16 \text{ mm} \leq s \leq 20 \text{ mm}. \end{cases} \tag{15}$$

Generally, the optimal design for the MOD problem cannot be found. Thus, the design task is now to seek for the Pareto optimal front among the design space. Modified NSGA-II algorithm (Deb et al. 2002) is chosen to search for the Pareto front of the contradictory objectives  $M^*$  and  $M_d$ . According to design requirements, the optimal design must be chosen based on the Pareto front.

#### 5.2 Results and discussion

The MOD problems of the DLTS hinge under pure bend loading are analyzed based on corresponding RS models. NSGA-II is employed to find the optimal solutions with a population size of 100 and a generation number of 120. The value of the objective function is calculated as the sum of all optimization objective components ( $OBJ_k$ ) with a corresponding weight factor ( $W_k$ ) and scale factor ( $S_k$ ) of the  $k$ -th objective component:

$$\text{Objective} = \sum_{k=1}^q \frac{OBJ_k \times W_k}{S_k} \tag{16}$$

where  $k$  ( $k=1, 2, \dots, q$ ) is the number of the optimization objectives, and  $q$  ( $q=2$ ) is the total number of optimized objectives.

If the weight and scale factors of the objective component are equal and the order of magnitude of the objective component vary considerably. Then the effect of the component with a small magnitude weakens. Thus, the scale factor of  $M^*$  and  $M_d$

**Table 9** The first optimal design of the DLTS hinge with  $S_m \leq 0.6\text{GPa}$

| $s$ (mm) | $\varphi$ (deg) | $R$ (mm) | $S_m$ (Gpa) |       |        | $M_d$ (Nm) |       |        | $M^*$ (Nm) |       |        |
|----------|-----------------|----------|-------------|-------|--------|------------|-------|--------|------------|-------|--------|
|          |                 |          | RS model    | FEA   | RE (%) | RS model   | FEA   | RE (%) | RS model   | FEA   | RE (%) |
| 19.490   | 83.619          | 20.878   | 0.572       | 0.571 | 0.939  | 1.336      | 1.413 | -5.78  | 0.182      | 0.172 | 5.45   |

**Table 10** The second optimal design of the DLTS hinge with  $S_m \leq 0.6$  GPa

| $s$ (mm) | $\varphi$ (deg) | $R$ (mm) | $S_m$ (Gpa) |       |        | $M_d$ (Nm) |       |        | $M^*$ (Nm) |       |        |
|----------|-----------------|----------|-------------|-------|--------|------------|-------|--------|------------|-------|--------|
|          |                 |          | RS model    | FEA   | RE (%) | RS model   | FEA   | RE (%) | RS model   | d     | RE (%) |
| 19.844   | 84.698          | 17.046   | 0.563       | 0.549 | 2.59   | 1.408      | 1.514 | 7.68   | 0.191      | 0.182 | 4.49   |

are set as 0.1 and 1.0, respectively, i.e.,  $S_1=0.1$  and  $S_2=1.0$ . The weight factor of  $M^*$  and  $M_d$  are all set as 1.0, i.e.,  $W_1=W_2=1.0$ . The Pareto fronts for the quasi-static deployment optimization problems of the DLTS hinge as defined in Eq. (15) are obtained and plotted in Fig. 13. The shaded area in the Pareto front is feasible region. If the designs are located in the outside of the shaded area, such as points  $p$ ,  $q$  and  $t$ , these are not the optimal design. From the Fig. 13, it is revealed that  $M^*$  and  $M_d$  are negatively correlated with the  $S_m$ , which is less than 0.6GPa. Thus, the driving moment  $M^*$  increases as the locking moment  $M_d$  decreases.

The two single-objective optimization design (SOD) are the limiting points of the Pareto curve. These designs are located at each end of the Pareto curve and are marked as a red solid five-point star in Fig. 13. The optimum hinge configurations and corresponding ideal optimal designs of the two single objective functions  $M^*$  and  $M_d$  are depicted in Table 8. Two optimums with different section radii and central angles are found in the same large tape-spring separation distance of  $s=20$ .

According to practical application conditions, two of the optimum designs are obtained as listed in Tables 9 and 10. The FE models for the optimal design configuration are also established, as depicted in these tables.  $M^*$  is lower than 0.18 Nm for the first optimal design configuration. Thus, this optimal design configuration cannot be selected. However, for the second optimal design configuration all three features are suitable for the optimal model as depicted in Eq. (15). Both the response surface and the finite element results for the second optimum design are located in the shaded area. And the REs between the RS models and the FEA results are also not more than 7.68 % which demonstrates the accuracy of the surrogate models. Thus, the second optimal design configuration is selected as the last optimal design parameters, i.e.,  $s=19.844$  mm,  $R=17.046$  mm, and  $\varphi=84.698^\circ$ .

## 6 Conclusions

This paper has presented a detailed study of the quasi-static folding and deployment of the tape-spring hinge using numerical method, experiments and the response surface method. The numerical models are established for a particular DLTS hinge and the corresponding moment-rotation profile during quasi-static deployment is measured starting from the complete

folded configuration. One of the main contributions of this study is validation of the numerical models for the tape-spring hinges through the experiment data. The qualitative comparison of the deformation configuration shows that both entire geometric configurations and the positions of the localized deformation regions in a DLTS hinge are in good accordance with each other. In addition, the comparison between the measured and predicted moment-rotation profiles during the quasi-static deployment of the DLTS hinge has shown good qualitative agreement. However, the main area of quantitative discrepancy is the profile slope from the peak moment to the steady-state moment. This discrepancy is caused by two reasons: one reason is that the rigid clamp ends and the rigid clamp holders enhance the bend stiffness of the DLTS hinges; another reason is that the deployment test of the DLTS hinges has a small angle twist caused by installation or manufacturing errors.

DLTS hinges are selected as a better configuration compared to the behavior of the single-layer tape-spring (SLTS) hinge. The numerical results indicate that both  $M_d$  and the  $M^*$  of the DLTS hinge are two times as that of the SLTS hinge, but the  $S_m$  of the DLTS hinge is less than that of the SLTS hinge for all tape-spring hinge configurations. The numerical results indicate that the DLTS hinge has better deployment capacity and lower stress concentration compared with SLTS hinge.

The most important contribution of this paper is that the optimal design is obtained using the validated numerical model and the response surface method. The multiobjective optimization design (MOD) has been implemented by employing a surrogate model and the modified non-dominated sorting genetic algorithm NSGA-II algorithm. The quadratic polynomial functions are chosen to construct the RS models. The surrogate models of  $S_m$ ,  $M^*$ , and  $M_d$  are established for the DLTS hinge based on the three-level full factorial design of experiments method. The Pareto front of the MOD for the DLTS hinge that contains a range of optimal designs is obtained. The values of the driving moment  $M^*$  and the locking moment  $M_d$  are negatively correlated with the maximum stress  $S_m$ , which is less than 0.6GPa. Thus, the driving moment  $M^*$  increases as the locking moment  $M_d$  decreases.

**Acknowledgments** This project is supported by the College Discipline Innovation Wisdom Plan in China (Grant No. B07018), the Self-Planned Task (No.SKLR201401A02) of State Key Laboratory of Robotics and System (HIT), and the Fundamental Research Funds for the Central Universities (No.HIT.NSRIF.2015050). This support is gratefully acknowledged by the authors.

## References

- Block J, Straubel M, Wiedemann M (2011) Ultralight deployable booms for solar sails and other large gossamer structures in space. *Acta Astronaut* 68(7–8):984–992
- Boesch C, Pereira C, John R, Schmidt T, Seifart K, Sparr H, Lautier JM, Pyttel T (2008) Ultra light self-motorized mechanism for deployment of light weight space craft appendages. 39th aerospace mechanisms symposium 7–9 May 2008, Newport, NASA Marshall Space Flight Center
- Box GEP, Wilson KB (1951) On the experimental attainment of optimum conditions. *J Roy Stat Soc* 13:1–45
- Deb K, Pratap A, Agarwal S, Meyarivan T (2002) A fast and elitist multiobjective genetic algorithm: NSGA-II. *IEEE Trans Evol Comput* 6(2):182–197
- Hou SJ, Dong D, Ren LL, Han X (2012) Multivariable crashworthiness optimization of vehicle body by unreplicated saturated factorial design. *Struct Multidiscip Optim* 46:891–905
- Hou SJ, Liu TY, Dong D, Han X (2014) Factor screening and multivariable crashworthiness optimization for vehicle side impact by factorial design. *Struct Multidiscip Optim* 49:147–167
- Li M, Deng ZQ, Liu RQ, Guo HW (2011) Crashworthiness design optimization of metal honeycomb energy absorber used in lunar lander. *Int J Crashworthines* 16(4):411–419
- Lindman HR (1992) *Analysis of variance in experimental design*. Springer, New York
- Liu YH, Day ML (2008) Bending collapse of thin-walled circular tubes and computational application. *Thin-Walled Struct* 46(4):442–450
- Mallikarachchi HMYC, Pellegrino S (2010) Optimized designs of composite booms with integral tape-spring hinges. 51st AIAA/ASME/ASCE/AHS/ASC structures, structural dynamics, and materials conference 12–15 April 2010, Orlando, Florida
- Mallikarachchi HMYC, Pellegrino S (2011) Quasi-static folding and deployment of ultrathin composite tape-spring hinges. *J Spacecr Rocket* 48(1):187–198
- Mansfield EH (1973) Large-deflexion torsion and flexure of initially curved strips. *Proc R Soc Lond A Math* 334(1598):279–298
- Marks GW, Reilly MT, Huff RL (2002) The lightweight deployable antenna for the MARSIS experiment on the mars express spacecraft. 36th aerospace mechanisms symposium 14–17 May 2002. Cleveland, Ohio
- Mobrem M, Adams DS (2009) Deployment analysis of lenticular jointed antennas onboard the mars express spacecraft. *J Spacecr Rocket* 46(2):394–402
- Oya K, Onoda J (2002) Characteristics of carpenter tape hinge made of TiNi alloy. 43rd AIAA/ASME/ASCE/AHS/ASC structures, structural dynamics, and materials conference 22–25 April 2002, Denver, Colorado
- Qi C, Yang S, Dong FL (2012) Crushing analysis and multiobjective crashworthiness optimization of tapered square tubes under oblique impact loading. *Thin-Walled Struct* 59:103–119
- Seffen KA (2001) On the behavior of folded tape-springs. *J Appl Mech T ASME* 68(3):369–375
- Seffen KA, Pellegrino S (1999) Deployment dynamics of tape springs. *Proc R Soc Lond A* 455:1003–1048
- Seffen KA, You Z, Pellegrino S (2000) Folding and deployment of curved tape springs. *Int J Mech Sci* 42:2055–2073
- Silver MJ, Hinkle JD, Peterson LD (2004) Modeling of snap-back bending response of doubly slit cylindrical shells. 45th AIAA/ASME/ASCE/AHS/ASC structures, structural dynamics, and materials conference 19–22 April 2004, Palm Springs, Calif
- Silver M, Hinkle JD, Peterson LD (2005) Controlled displacement snap-through of tape springs: modeling and experiment. 46th AIAA/ASME/ASCE/AHS/ASC structures, structural dynamics & materials conference 18–21 April 2005, Austin, Texas
- Soykasp O, Pellegrino S, Howard P, Notter M (2008) Folding large antenna tape spring. *J Spacecr Rocket* 45(3):560–567
- Watt AM, Pellegrino S (2002) Tape-spring rolling hinges. 36th aerospace mechanisms symposium 15–17 May 2002, Cleveland, OH
- Yang H, Deng ZQ, Liu RQ, Wang Y, Guo HW (2014) Optimizing the quasi-static folding and deploying of thin-walled tube flexure hinges with double slots. *Chin J Mech Eng* 27(2):279–286
- Yee JCH (2006) *Thin CFRP Composite Deployable Structures*, PhD thesis, University of Cambridge
- Yee JCH, Pellegrino S (2005) Composite tube hinges. *J Aerosp Eng* 18:224–231